Kobe University Repository : Kernel

PDF issue: 2024-05-21

Wavelength-dependent near-infrared microbolometer for short-wavelength infrared light with gold nanowire grating optical absorber

Tsubota, Tatsuya
Uesugi, Akio
Sugano, Koji
Isono, Yoshitada

(Citation)
Microsystem Technologies,27(3):997-1005

(Issue Date)
2021-03

(Resource Type)
journal article

(Version)
Accepted Manuscript

(Rights)
© Springer-Verlag GmbH Germany, part of Springer Nature 2020. This version of the article has been accepted for publication, after peer review (when applicable) and is subject to Springer Nature's AM terms of use, but is not the Version of Record and does not reflect post-acceptance improvements, or any corrections. The Version of…

(URL)
https://hdl.handle.net/20.500.14094/90008038

Title page

The names of the authors Tatsuya Tsubota, Akio Uesugi, Koji Sugano, Yoshitada Isono

Title Wavelength-dependent near-infrared microbolometer for short-wavelength infrared light with gold nanowire grating optical absorber

Affiliation of the authors Department of Mechanical Engineering, Graduate School of Engineering, Kobe University, Kobe, Hyogo 657-8501, Japan

Corresponding authors Tatsuya Tsubota 209t346t@stu.kobe-u.ac.jp, Koji Sugano sugano@mech.kobe-u.ac.jp

ORCID Akio Uesugi: https://orcid.org/0000-0002-7913-3679, Koji Sugano: https://orcid.org/0000-0002-0780-0110, Yoshitada Isono: https://orcid.org/0000-0003-2370-3246

Abstract

Near-infrared (NIR) imaging has been used for nondestructive and non-contact inspections in various areas, such as food and medicine inspections and medical diagnoses. The short-wavelength infrared light (SWIR) sensor currently used requires a Peltier cooler and a diffraction grating spectroscope owing to its detection principle. Thus, realizing a low-cost and miniaturized SWIR imaging device remains challenging and has limitations for practical applications. In this study, we propose a bolometer-type detector element fabricated using a silicon-on-insulator (SOI) wafer as a low cost and miniaturized SWIR image sensor element. We adopted gold (Au) nanowire grating structures coated with silicon as wavelength-dependent SWIR absorbers and aimed at wavelength-selectivity imaging without using a spectroscope. A device was designed and fabricated with Au nanowire grating structures on a doubly clamped Si beam using microelectromechanical system (MEMS)) technology. The electrical characteristics of the device were measured depending on device temperature and SWIR irradiation intensity. It was found that electrical resistance decreased linearly with increasing device temperature and SWIR irradiation intensity (wavelength at 1530 nm), as semiconductors have negative temperature coefficients of resistance. The results show similar trends from both finite element method (FEM) analysis and theoretical calculation. The resistances at wavelengths ranging from 1530 to 1565 nm at 5 nm increment were evaluated. It was confirmed that absorber-integrated bolometer device enabled wavelength-dependent response of the resistance according to the absorption spectrum.

Declarations

Funding The project was also funded by the Ministry of Education, Culture, Sports, Science, and Technology (MEXT), Japan. A part of this study was supported by JSPS KAKENHI Grant Number JP18H01847 and 19H02571.

Conflicts of interest The authors declare that they have no conflict of interest.

Availability of data and material (data transparency) The datasets generated during and/or analyzed during the current study are available from the corresponding author on reasonable request.

Code availability (software application or custom code) Not applicable

Acknowledgments

A part of this study was supported by the Micro/Nano Fabrication Hub in Kyoto University and Nanotechnology Open Facilities in Osaka University. The project was also funded by the Ministry of Education, Culture, Sports, Science, and Technology (MEXT), Japan. A part of this study was supported by JSPS KAKENHI Grant Number JP18H01847 and 19H02571.

Text

1. Introduction

A near-infrared (NIR) detector that enables nondestructive and non-contact inspection has been recently used in various applications, such as in food (ElMasry et al. 2012; Jiang et al. 2016; Lee et al. 2014; Wu and Sun 2013) and medicine inspections (Andre 2003) and for medical diagnoses (Koizumi et al. 1999; Luo et al. 2011). The detectors currently marketed for short-wavelength infrared light (SWIR, wavelength range: 1–3 μm) are known as photodiodes, which are fabricated from InGaAs (Yuan et al. 2007) or InAs (Marshall et al. 2008) using a photoelectric effect. They have excellent responsiveness and detection sensitivity; however, they require a Peltier cooler to reduce the dark current of the photoelectric effect. Furthermore, they also require a diffraction grating spectroscope for hyperspectral imaging, making their cost reduction and miniaturization challenging. Thus, they can be limited for practical applications (Manley 2014; Nicolaï et al. 2007).

For the detection of mid-wave infrared light (MWIR, wavelength range: 3–5 μm) and long-wave infrared light (LWIR, wavelength range: 8–14 μm), various studies on photon and thermal detectors have been conducted. Thermal detectors utilize the temperature change of the detection elements due to infrared absorption. Recently, thermal detectors have opened new opportunities for military and commercial applications owing to their small size, light weight, low power consumption, and wideband wavelength detection capability, compared to photon detectors (Bhan et al. 2009; Kimata 2018; Tezcan et al. 2001).

In particular, the recent advances in microelectromechanical system (MEMS) technology allow fabrication of sensitive thermal microbolometer, which is common in thermal detection technologies currently available. Bolometers measure changes in infrared radiation intensity and convert it into an electrical resistance change. Bolometers absorb infrared radiation, thus resulting in an electrical resistance change due to an increase in temperature. They are normally integrated with CMOS (Complementary metal-oxide-semiconductor) circuits to achieve higher sensitivity and smaller pixel size than with other thermal sensors, such as thermoelectric (Oliver and Wise 1999) and SOI diode detectors (Tanaka et al. 1992). Thus, they are widely used for security, night vision, and autonomous driving (Kimata 2018) in MWIR and LWIR applications.

Numerous materials have been studied for bolometers such as metals (gold (Au), platinum, titanium) and semiconductors (vanadium oxide (Bonora et al. 2010), amorphous silicon (Bain et al. 2000)). In bolometers, the temperature coefficient of resistance (TCR) is an important parameter. Metals typically have positive TCR and their resistance increases with increasing temperature. In contrast, semiconductors have negative TCR and their resistance decreases with increasing temperature. The TCR values of semiconductors are larger than those of metals, thus small temperature changes can be detected.

Recently, advanced functional sensors with wavelength-selectivity for identification of substances through their emission spectra in the MWIR and LWIR regions have been drawing significant attention. A spectroscope is required to realize wavelength-selectivity; however, this not only leads to high cost and large device size but also increases noise as it emits infrared radiation to the sensor (Ogawa et al. 2018). To address this challenge, studies on various structures with wavelength-dependent, such as plasmonic crystals (Ogawa et al. 2012) and metal insulator metal (MIM) (Hao et al. 2010) have been performed (Ogawa et al. 2019). As described above, research on MWIR and LWIR detections has been conducted; however, no research on thermal sensors for SWIR detection has been reported.

Therefore, a bolometer-type detector as an SWIR image sensor for low cost and miniaturization (by removing the Peltier cooler and spectroscope) has been proposed in this study, as shown in Figure 1. This device can be easily

fabricated using MEMS technology from an SOI wafer. In this device, SWIR radiation heats the absorber on the Si fixed beam, which in turn changes its resistance with respect to its TCR value. This detector uses Au nanowire grating structures coated with silicon as a wavelength-dependent SWIR absorber for multi-wavelength imaging without using a spectroscope. Surface plasmon resonance (SPR) can be coupled with nanowire grating structures whose period is around the wavelength of the incident light (Chen et al. 2016; Ongarello et al. 2011; Zilio et al. 2010). Localization of SPR also occurs, which results in an electric field enhancement. This phenomenon leads to a strong absorption of incident light at a specific wavelength band on a nanoscale metal structure. The absorption peak wavelength of the plasmonic structure also depends on the surrounding refractive index. Thus, the Au nanowire grating structures are coated with Si, which has high refractive index and excellent integration with MEMS fabrication processes. By adopting the above structures, an absorber with a sharp absorption peak in the SWIR region can be fabricated. The optical characteristics of the plasmonic structures can be controlled by their material, structure, and size (Li et al. 2014). In this study, we focused on the optical characteristics when the lattice spacing of the Au nanowire grating structures was changed to easily fabricate the devices with multiple absorption spectra on one SOI wafer. It was assumed that by arraying elements with different absorption wavelength bands, spectral information of incident light can be obtained.

In this study, fabrication and evaluation of microbolometer devices integrated with a wavelength-dependent SWIR absorber were carried out. The absorption spectra of the fabricated absorbers were measured, which have different grating period of Au nanowires to control the wavelength of the absorption peaks. The electrical characteristics were also measured at various device temperatures, light intensities, and wavelengths. The characteristics of an absorber-integrated bolometer device that focuses on wavelength-dependent response according to the absorption spectrum with small absorption change is reported in this paper.

2. Measurement principle

2.1 Device structures

For the bolometer proposed in this study, the light intensity P is measured based on the change in the electrical resistance ΔR of the doubly clamped Si beam, which is caused by the temperature change ΔT when the absorber at the center of the Si beam is irradiated with light. A schematic image of the device is shown in Fig. 1. To obtain high sensitivity, the bolometer was designed in such a way that heat loss is suppressed. In particular, the heat conduction from the Si beam to the substrate layer has a serious negative influence on the performance of the bolometer. Hence, the device has a through hole to reduce heat loss from the beam. The elements that determine the electrical resistance and temperature of the device are divided into three parts: the center pad with the Si absorber, the freestanding Si beam, and the subsequent fixed Si beam on the buried-oxide (BOX) layer, as shown in Fig. 1. The electrical resistance is determined by their sum. The center pad with an optical absorber is supported by narrow Si beams fixed at both ends, indicating the freestanding structure. The freestanding length of the Si beam from the edge of the center pad to the edge of the through hole was 500 μm. The width and thickness of the freestanding Si beam were 10 and 1.5 μm, respectively. The electrical resistance of the Si beam was measured via electrode pads fabricated on both sides.

2.2 Theory

The important figure of merit for the resistance bolometer is a temperature coefficient of resistance (TCR) α defined as follows:

$$\alpha = \frac{1}{R_0}\frac{\Delta R}{\Delta T} \tag{1}$$

where R_0 is the initial electrical resistance. While a Si beam with a uniform cross-section and a length of $2l$ is considered as a simple model, the temperature distribution in the longitudinal direction of the beam $dT(x)/dx$ can be derived by solving the one-dimensional Fourier law as follows:

$$\frac{dT(x)}{dx} = -\frac{\beta P}{2bh\kappa} \tag{2}$$

where κ, P, and β denote the thermal conductivity, irradiating light intensity to the absorber, and wavelength-dependent light absorption rate, respectively. The width and thickness of the Si beam are represented by b and h, respectively. The average temperature change of the Si beam ΔT can be obtained by integrating the length of the Si beam $2l$ as follows:

$$\Delta T = \frac{1}{2l}\int_{-l}^{l}\left\{-\frac{\beta P}{2bh\kappa}(|x-l|)\right\}dx = \frac{l}{4bh\kappa}\beta P \tag{3}$$

Thus, the resistance change ΔR can be expressed as a function of the temperature change of Si beam ΔT and the light intensity P as follows:

$$\Delta R = \alpha \Delta T R_0 = \frac{\alpha l R_0}{4bh\kappa}\beta P \tag{4}$$

3. Analytical and experimental methods

3.1 Analytical method

To investigate the influence of light intensity on the temperature of the device, thermal analysis was performed using the finite element method (FEM). The design dimensions shown in Fig. 1 were used for the analytical model. The temperature at the bottom of the substrate was fixed at the initial temperature of 27 ºC. A heating area of 20 μm × 20 μm, which is equal to the dimension of the absorber, was set at the center. The absorption rate was assumed to be 43.2% based on the measurement results of the absorption of the Au nanowire grating structures shown in Sec. 4.3. A heat quantity ranging from 0.000 to 0.432 mW was applied to the heating area for the analysis, corresponding to a light intensity ranging from 0.0 to 1.0 mW considering an absorption of 43.2%. A theoretical calculation was also performed using Eq. (3) to obtain the average temperature of the Si beam.

3.2 Device fabrication

An SOI wafer with a device layer thickness of 1.5 μm, a BOX layer thickness of 0.25 μm, and a Si substrate thickness of 540 μm was used for device fabrication. First, chromium (Cr) masks for the through hole, which were made through Deep-RIE (reactive ion etching), were fabricated on the back surface of the substrate using Cr vacuum deposition, photolithography, and Cr etching. Aluminum (Al) patterns of electrodes with dimensions 250 μm × 250 μm and absorbers with dimensions 30 μm × 30 μm were fabricated on the front surface of the device layer using Al vacuum deposition, photolithography, and Al etching. Then, they were annealed to obtain an ohmic junction at the interface between Si and Al. Subsequently, the Al patterns were overlaid with the Au patterns of electrodes and absorbers using photolithography, Au vacuum deposition, and lift-off processes. The Au nanowires were arranged on the Au thin film with lines and spaces and fabricated using electron-beam (EB) lithography, Au deposition, and lift-off processes. The Au nanowires, each with a width of 100 nm, a height of 50 nm, and a grating period of 400–800 nm, were fabricated. Then Au nanowires were coated with Si by sputtering to obtain an absorption peak in the near-infrared wavelength. The coating Si thickness was 100 nm. After the through hole was fabricated using Deep-RIE, the sputtered Si and the beam were patterned using

photolithography and subsequent Si dry etching. Finally, the BOX layer was removed from the backside using buffered hydrofluoric acid.

3.3 Optical characterization

The absorption rate β [%] of the absorber is expressed as $\beta = 100 - T - R$, where T [%] and R [%] denote the transmittance and reflectance, respectively. It was assumed that $T = 0$ without considering transmission as the Au layer thickness of 100 nm was too thick to be penetrated. The reflectance was measured using a microscopic spectrometer (MSV-5200, JASCO) and calibrated using the reflectance of the Au film. The measurement wavelength ranged from 1000 to 1800 nm.

3.4 Bolometer characterization

The electrical characteristics of the fabricated devices were measured. First, the device electrodes were connected to the printed circuit board by Au wire bonding. The electrical current was measured while a DC voltage was applied between the electrodes using a DC power supply. The applied voltage was determined to be 0.3 V, which produced small noise and Joule heat effects based on the preliminary experiments. A Peltier device was set under the bolometer chip to control the device temperature by 1°C from 27 to 40°C. The near-infrared was irradiated onto the absorber placed on the Si beam by selecting the intensity and wavelength using a wavelength-tunable laser. The output wavelength of the laser used in this study ranged from 1530 to 1565 nm. The intensity was adjusted between 0.240 and 0.485 mW. To reduce electrical noise and external light, the device was placed in an Al case.

4. Results and discussions

4.1 Analytical

Figures 2(a) – (b) show the FEM analytical results of the device temperature distribution when a heat quantity of 0.432 mW was applied. Figure 2(b) shows the temperature distribution in the longitudinal direction. The temperature in the center-pad region was almost constant because of its high thermal conductivity owing to its large cross-sectional area. The temperature of the freestanding-beam region decreased along the longitudinal direction according to the Fourier law shown in Eq. (2). For the fixed-beam region, it was confirmed that the temperature at the fixed end of the beam did not change due to heat conduction to the substrate. The average temperature changes in the center pad, freestanding beam, and fixed-beam regions were 46.3, 23.1, and 0.025°C, respectively. The temperature change in the fixed-beam region could be considered negligible as it was significantly smaller than that of the freestanding-beam region. The resistance of the fixed Si beam was thought not to change.

Figure 2(c) shows the average temperature in the freestanding-beam region calculated using the FEM analysis and Eq. (3). From the analytical result, it was found that the temperature of the freestanding Si beam increased linearly in proportion to the light intensity as the amount of heat transferred to the Si beam increased with light intensity. Therefore, this confirms the validity of the theoretical calculation as its result agreed well with that of the FEM analysis.

4.2 Device fabrication

Figure 3 shows the scanning electron microscopy (SEM) image of the fabricated device. As we designed, a freestanding Si beam was successfully fabricated from an SOI wafer as shown in Fig. 3(a), integrating the Au nanowire grating structure at the center of the beam as an optical absorber as shown in Figs. 3(b) and (c). The measured lengths of the

freestanding Si beam and the fixed Si beam on the BOX layer were 500 and 50 μm, respectively. The measured width of the beams was 10 μm.

4.3 Optical characterization

Figure 4 shows the measured optical absorption spectra after fabrication of the Au nanowire grating structures. It was confirmed that the absorber with Si-deposited grating gold nanowires had absorption peaks in the SWIR wavelength range. This was based on the result of the absorber, which shows that only the sputtered Si without Au nanowire structure and Au nanowire grating structure without sputtered Si had no large peaks. The sputtered Si produced a broad peak at around 1700 nm because of the interference at the interfaces of the sputtered Si thin film. The absorber with a grating period of p = 400 nm had its first absorption peak at 1292 nm and second peak at 1472 nm. The absorber with a grating period of p = 500 nm had its first peak at 1366 nm and second peak at 1675 nm. In addition, the absorber with a grating period of p = 600 nm had its first peak at 1377 nm and second peak at 1771 nm. These results confirm that both the first and second absorption peaks shifted to longer wavelengths as the grating period increased. The absorbers with grating periods of 700 and 800 nm had single peak as the second peak was assumed to appear at wavelengths longer than 1800 nm. An absorber with a single peak in the SWIR wavelength is desirable for obtaining an intensity measurement at each wavelength band without using a spectroscope. In the future, it will be necessary to optimize the structures and dimensions of the absorbers for obtaining the desired absorption characteristics.

4.4 Bolometer characterization

Figure 5 shows the current-voltage (IV) measurement results of the fabricated devices. Ohmic junction characteristics can be obtained by annealing the interface between Al and Si at the electrode pads.

Figures 6(a) and (b) show the measured resistance for a grating period of p=400 nm as a function of the device temperature controlled by the Peltier device and the light intensity, respectively. The wavelength used in this measurement was 1530 nm. It was found that resistance decreased linearly with device temperature and light intensity. This result shows similar pattern as that of the theoretical calculation in Eq. (4) as the TCR values of semiconductors, such as Si, are negative and can be considered constant in small temperature changes. From Fig. 6(a), the measured resistances at 27 and 40°C were 51.9 and 43.8 MΩ, respectively, characterized by a linear relationship and which resulted in a TCR value of −0.012 /°C as calculated using Eq. (1). In this case, the temperature of the Si beam was considered constant as the device chip was heated from the backside using the Peltier device. The resistance of 52.3 MΩ without light irradiation decreased linearly to 48.6 MΩ at a light intensity of 0.485 mW.

The temperature change as a function of light intensity was calculated based on Figs. 6(a) and (b). The resistance change of the device under light irradiation was determined from the sum of the resistance changes of the three parts: the center pad, the freestanding-beam, and the fixed-beam regions. Both resistance changes of the center pad and the fixed-beam regions were negligible as the resistance and temperature changes were significantly smaller than those of the freestanding-beam region. The resistance of the center-pad region and the temperature change of the fixed-beam region were hundred-times and 940-times smaller than those of the freestanding-beam region, respectively. Thus, the resistance change was determined only from the freestanding-beam region using the following equation:

$$\Delta R = \alpha \Delta T_b R_{b0} \quad (5)$$

Here, ΔT_b and R_{b0} are the temperature change and initial resistance of the freestanding-beam region, respectively. ΔT_b can be calculated using Eq. (5) and the experimental α and ΔR. Figure 6(c) shows the relationship between the light intensity and the temperature of the freestanding Si beam calculated using Eq. (5) and based on the measurement results shown in Figs. 6(a) and (b). It was found that the temperature of the freestanding Si beam increased linearly with

light intensity by the photothermal conversion of the absorber. The calculated temperature of freestanding Si beam under 0.485 mW laser irradiation was 6.5°C. The reason for this smaller temperature change compared to the 23.1°C from the FEM analysis shown in Fig. 2(d) could be the large heat dissipation effect due to transfer to the atmosphere, which was not considered in the analysis. Therefore, measurements in vacuum are required in the future to improve the sensitivity.

This paragraph discusses the dependency of resistance change on laser wavelength. Assuming the temperature change of freestanding Si beam due to absorption of light is small, the temperature coefficient of resistance α can be regarded constant. Thus, sensitivity $\Delta R/P$ is proportional to freestanding Si beam temperature change ΔT_b and light absorption rate β, which depends on wavelength. In this study, we focused on the dependence of light absorption rate β on sensitivity. To compare sensitivity with absorption rate β as a function of wavelength λ, the normalized sensitivity and the normalized absorption rate were calculated using the following equations:

$$S(\lambda) = \left(\frac{\Delta R_\lambda}{P_\lambda}\right) \Big/ \left(\frac{\Delta R_{1530\mathrm{nm}}}{P_{1530\mathrm{nm}}}\right) \quad (6)$$

$$A(\lambda) = {\beta_\lambda}/{\beta_{1530\mathrm{nm}}} \quad (7)$$

where $S(\lambda)$ and $A(\lambda)$ denote the normalized sensitivity and normalized absorption rate based on the wavelength of $\lambda = 1530$ nm, respectively.

Figures 7(a) and (b) show the sensitivity and absorption rate of the two devices at p=400 nm and 800 nm and at wavelengths ranging from 1530 to 1565 nm. Figures 7(c) and (d) show the relationship between normalized sensitivity and normalized absorption rate. The absorption rate at p=400 nm tended to increase from 43.2% to 44.7% as the wavelength increased from 1530 to 1565 nm as shown in Fig. 7(a), corresponding to the normalized absorption rate $A(\lambda)$ from 1.0 to 1.03 in Fig. 7(c). In contrast, the absorption at p=800 nm tended to decrease from 60.1% to 52.8% as the wavelength increased from 1530 to 1565 nm as shown in Fig. 7(b), corresponding to the normalized absorption $A(\lambda)$ from 1.0 to 0.88 in Fig. 7(d). We chose these devices to investigate the dependency of wavelength-dependent absorption on relative sensitivity. The resistance changes at p = 400 and 800 nm are shown in Figs. 7(a) and (b), respectively, also exhibit increasing and decreasing relationships with wavelength, respectively. Although the two devices showed both increasing and decreasing absorption trends, the trends for the normalized sensitivity $S(\lambda)$ and normalized absorption $A(\lambda)$ are in good agreement as well as those values. Depending on the wavelength, the small $S(\lambda)$ change of 1% or less matched well with $A(\lambda)$

It was confirmed that the absorber-integrated bolometer device enabled wavelength-dependent response according to the absorption spectrum and detection of small absorption change (1% or less) as the resistance changed. The developed devices could provide low-cost and miniaturized SWIR spectrometers.

5. Conclusion

This study proposed a bolometer-type detector element with wavelength-dependent fabricated from an SOI wafer as an SWIR image sensor element for low cost and miniaturization. Although bolometers have lower detection sensitivity compared to conventional photon detectors, they can be operated at room temperature and do not require Peltier coolers. In addition, it was expected that wavelength-selectivity imaging could be realized without a spectroscope by adopting Au nanowire grating structures that strongly absorb a specific wavelength of SWIR caused by surface plasmon resonance as the optical absorber. Devices with Au nanowire grating structures on a doubly clamped Si beam were fabricated using MEMS technology. It was confirmed that the fabricated Au nanowire grating structures had absorption peaks in the SWIR and the absorption peaks shifted to longer wavelengths as the grating period increased. To evaluate the proposed

1 devices, electrical characteristics at device temperatures ranging from 27 to 40°C at 1°C increment and SWIR light
2 intensity ranging from 0.240 to 0.485 mW were measured. It was found that electric resistance decreased linearly with
3 increasing temperature and light intensity and showed similar trends in both the theoretical calculation and FEM analysis.
4 In the future, measurement in vacuum is required to suppress heat loss and improve sensitivity as the experimental
5 temperature change was much smaller than the analytical result. The resistance at wavelengths ranging from 1530 to
6 1565 nm at 5 nm increments were evaluated. It was confirmed that the absorber-integrated bolometer device enabled
7 wavelength-dependent response according to the absorption spectrum and detection of small absorption change (1% or
8 less) as the resistance changed. It was shown that the device could serve as an SWIR imaging element without requiring
9 a spectroscope and a cooler, thereby reducing cost and size.

10 **References**

11 Andre M (2003) Multivariate analysis and classification of the chemical quality of 7-aminocephalosporanic acid using
12 near-infrared reflectance spectroscopy Anal Chem 75:3460-3467 https://doi.org/10.1021/ac026393x
13 Bain A et al. (2000) Amorphous silicon-based uncooled microbolometer technology for low-cost IRFPA Sensors and
14 materials 12:365-373
15 Bhan R, Saxena R, Jalwani C, Lomash S (2009) Uncooled infrared microbolometer arrays and their characterisation
16 techniques Defence Science Journal 59:580
17 Bonora S, Bortolozzo U, Residori S, Balu R, Ashrit PV (2010) Mid-IR to near-IR image conversion by thermally induced
18 optical switching in vanadium dioxide Opt Lett 35:103-105 https://doi.org/10.1364/OL.35.000103
19 Chen W, Kan T, Ajiki Y, Matsumoto K, Shimoyama I (2016) NIR spectrometer using a Schottky photodetector enhanced
20 by grating-based SPR Opt Express 24:25797-25804 10.1364/OE.24.025797
21 ElMasry G, Sun D-W, Allen P (2012) Near-infrared hyperspectral imaging for predicting colour, pH and tenderness of
22 fresh beef J Food Eng 110:127-140 https://doi.org/10.1016/j.jfoodeng.2011.11.028
23 Hao J, Wang J, Liu X, Padilla WJ, Zhou L, Qiu M (2010) High performance optical absorber based on a plasmonic
24 metamaterial Appl Phys Lett 96:251104 https://doi.org/10.1063/1.3442904
25 Jiang Y, Li C, Takeda F (2016) Nondestructive detection and quantification of blueberry bruising using near-infrared
26 (NIR) hyperspectral reflectance imaging Scientific Reports 6:35679 https://doi.org/10.1038/srep35679
27 Kimata M (2018) Uncooled infrared focal plane arrays IEEJ Transactions on Electrical and Electronic Engineering 13:4-
28 12 https://doi.org/10.1002/tee.22563
29 Koizumi H, Yamashita Y, Maki A, Yamamoto T, Ito Y, Itagaki H, Kennan RP (1999) Higher-order brain function
30 analysis by trans-cranial dynamic near-infrared spectroscopy imaging Journal of Biomedical Optics 4:403-414
31 https://doi.org/10.1117/1.429959
32 Lee W-H, Kim MS, Lee H, Delwiche SR, Bae H, Kim D-Y, Cho B-K (2014) Hyperspectral near-infrared imaging for
33 the detection of physical damages of pear J Food Eng 130:1-7 https://doi.org/10.1016/j.jfoodeng.2013.12.032
34 Li Z, Butun S, Aydin K (2014) Ultranarrow band absorbers based on surface lattice resonances in nanostructured metal
35 surfaces ACS nano 8:8242-8248 https://doi.org/10.1021/nn502617t
36 Luo S, Zhang E, Su Y, Cheng T, Shi C (2011) A review of NIR dyes in cancer targeting and imaging Biomaterials
37 32:7127-7138 https://doi.org/10.1016/j.biomaterials.2011.06.024
38 Manley M (2014) Near-infrared spectroscopy and hyperspectral imaging: non-destructive analysis of biological materials
39 Chem Soc Rev 43:8200-8214 https://doi.org/10.1039/c4cs00062e

Marshall ARJ, Tan CH, Steer MJ, David JPR (2008) Electron dominated impact ionization and avalanche gain characteristics in InAs photodiodes Appl Phys Lett 93:111107 https://doi.org/10.1063/1.2980451

Nicolaï BM, Beullens K, Bobelyn E, Peirs A, Saeys W, Theron KI, Lammertyn J (2007) Nondestructive measurement of fruit and vegetable quality by means of NIR spectroscopy: A review Postharvest Biology and Technology 46:99-118 https://doi.org/10.1016/j.postharvbio.2007.06.024

Ogawa S, Okada K, Fukushima N, Kimata M (2012) Wavelength selective uncooled infrared sensor by plasmonics Appl Phys Lett 100:021111 https://doi.org/10.1063/1.3673856

Ogawa S, Takagawa Y, Kimata M (2018) Broadband polarization-selective uncooled infrared sensors using tapered plasmonic micrograting absorbers Sensors and Actuators A: Physical 269:563-568 https://doi.org/10.1016/j.sna.2017.12.029

Ogawa S, Takagawa Y, Kimata M (2019) Elimination of Unwanted Modes in Wavelength-Selective Uncooled Infrared Sensors with Plasmonic Metamaterial Absorbers using a Subtraction Operation Materials 12 https://doi.org/10.3390/ma12193157

Oliver AD, Wise KD (1999) A 1024-element bulk-micromachined thermopile infrared imaging array Sensors and Actuators A: Physical 73:222-231 https://doi.org/10.1016/S0924-4247(98)00276-3

Ongarello T, Romanato F, Zilio P, Massari M (2011) Polarization independence of extraordinary transmission trough 1D metallic gratings Opt Express 19:9426-9433

Tanaka A, Suzuki M, Asahi R, Tabata O, Sugiyama S (1992) Infrared linear image sensor using a poly-Si pn junction diode array Infrared Phys 33:229-236 https://doi.org/10.1016/0020-0891(92)90019-P

Tezcan DS, Eminoglu S, Akar OS, Akin T A low cost uncooled infrared microbolometer focal plane array using the CMOS n-well layer. In: Technical Digest. MEMS 2001. 14th IEEE International Conference on Micro Electro Mechanical Systems, 2001. IEEE, pp 566-569. doi:https://doi.org/10.1109/MEMSYS.2001.906604

Wu D, Sun D-W (2013) Advanced applications of hyperspectral imaging technology for food quality and safety analysis and assessment: A review — Part II: Applications Innovative Food Science & Emerging Technologies 19:15-28 https://doi.org/10.1016/j.ifset.2013.04.016

Yuan Z, Kardynal B, Sharpe A, Shields A (2007) High speed single photon detection in the near infrared Appl Phys Lett 91:041114 https://doi.org/10.1063/1.2760135

Zilio P, Sammito D, Zacco G, Romanato F (2010) Absorption profile modulation by means of 1D digital plasmonic gratings Opt Express 18:19558-19565

1 # Figures

2

3

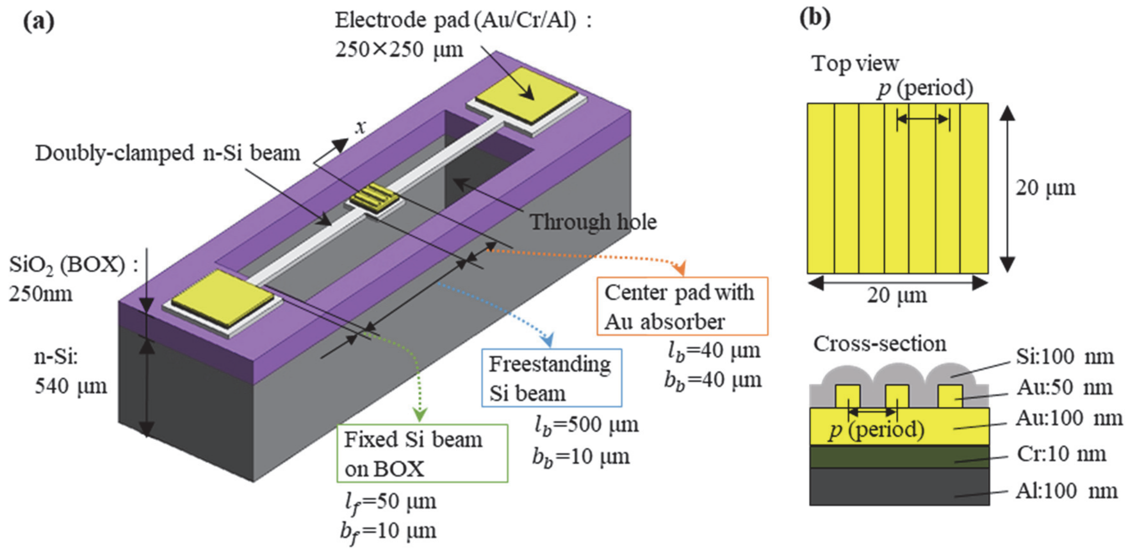

4

5 **Fig. 1** Bolometer-type SWIR detector device with an SWIR absorber fabricated using an SOI wafer. (a) Schematic
6 image of the detector. The freestanding Si beam was fixed at both ends. The absorber was located at the center pad of
7 the beam (40 μm×40 μm). The narrow Si beam for supporting the center pad was divided into freestanding Si beam and
8 fixed Si beam on the BOX layer, with lengths of 500 μm and 50 μm, respectively. (b) Schematic of the absorber with
9 gold nanowire grating structure covered with the sputtered Si thin film. The period was varied from 400 to 800 nm.

10

1

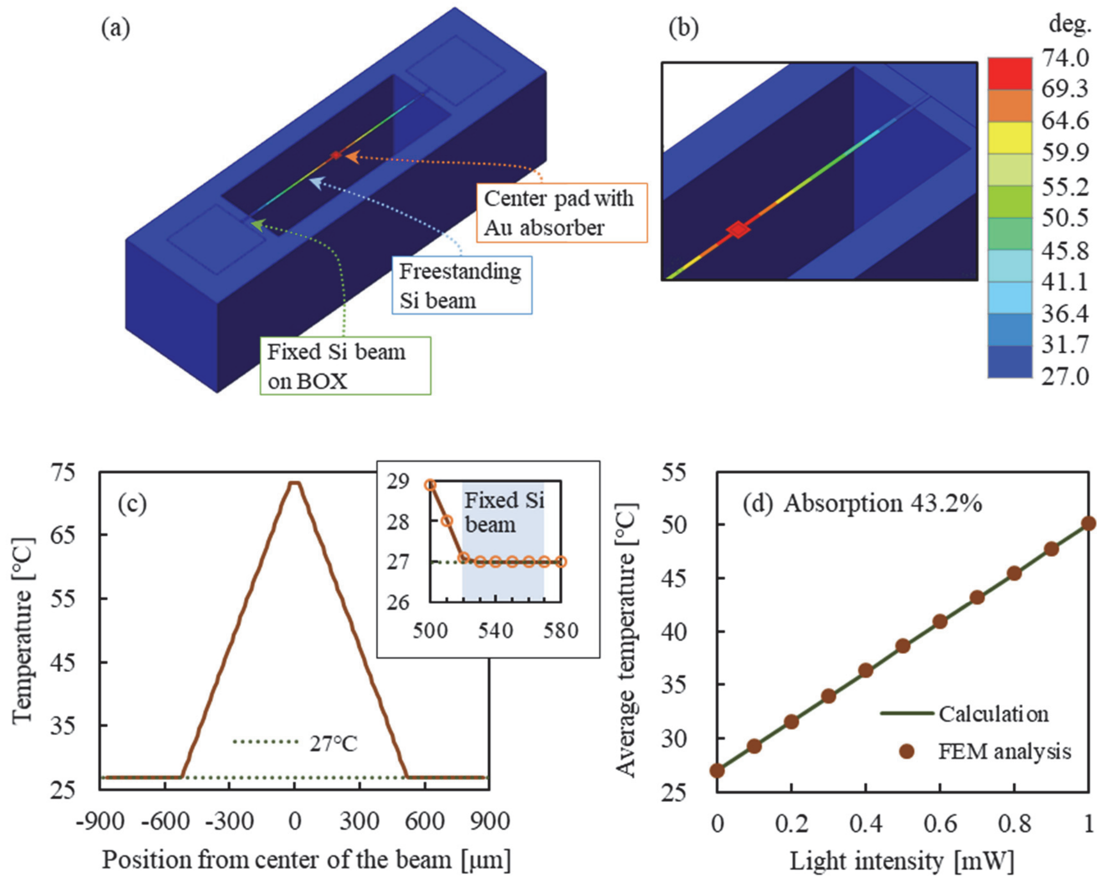

2

3 **Fig. 2** Analytical results (a), (b) Contour plot of the temperature of the fabricated device with 1 mW heat injection to
4 the Au absorber calculated through FEM simulation. Plot (b) shows the magnified image of (a). (c) Relationship between
5 beam position from the center of the beam and temperature at a light intensity of 1 mW calculated through FEM
6 simulation. (d) The average temperature of the Si beam with light intensity changing from 0 to 1 mW calculated through
7 FEM analysis and Eq. 3. The absorption was set at 43.2% in all calculations.

8

1

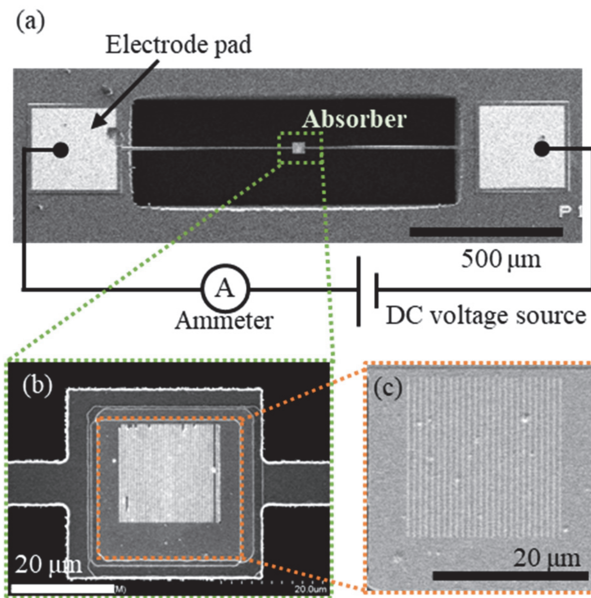

2

3 **Fig. 3** SEM images of the fabricated devices. (a) Freestanding Si beam fabricated from an SOI wafer. The Si beam is
4 connected to the ammeter and DC voltage source for electrical characterization. (b) Absorber at the center of the beam
5 (c) Absorber with the gold nanowire grating structures.

6

7

8

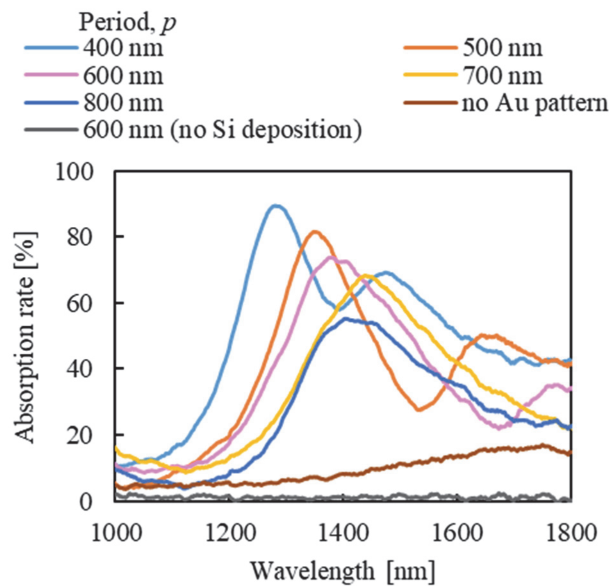

9

10 **Fig. 4** The measured optical absorption spectra of the gold nanowire grating structures with period (p) ranging from
11 400 to 800 nm. Absorption spectra for sputtered Si without gold nanowire structures and non-sputtered absorber with
12 period p = 600 nm are also shown.

13

1

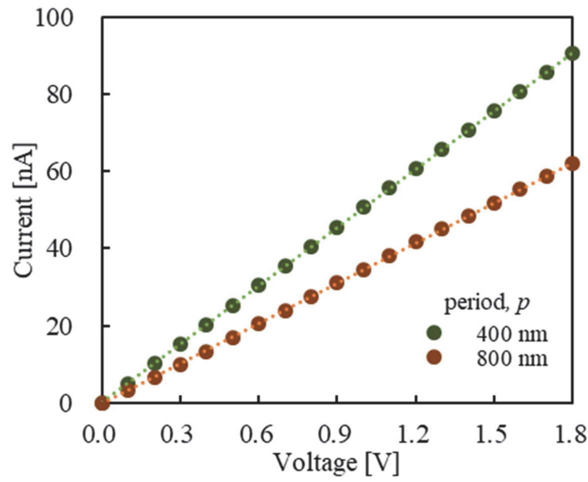

2

3 **Fig. 5** The measured current with applied DC voltage ranging from 0 to 1.8 V. Periods of 400 nm and 800 nm were
4 used for the Au nanowire grating structures.

5

6

7

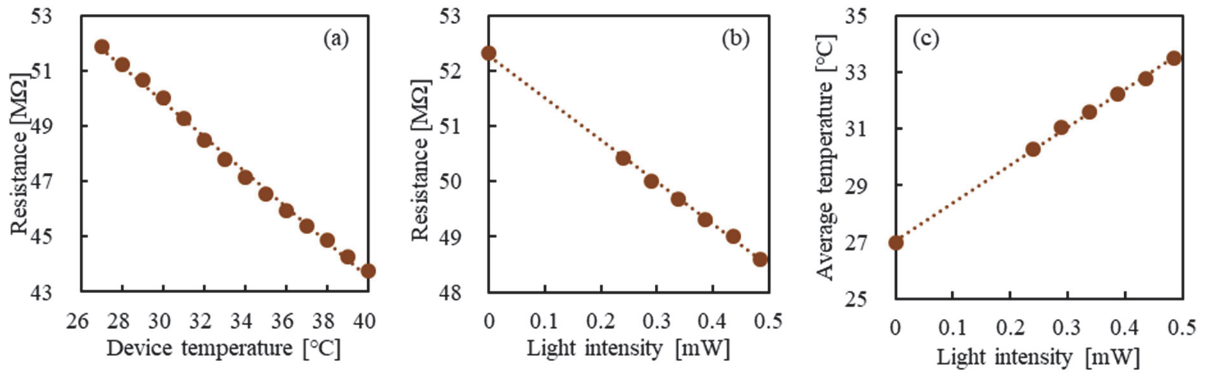

8

9 **Fig. 6** Electrical measurements for the device at a period of 400 nm. (a)Relationship between device temperature and
10 resistance with device temperature ranging from 27°C to 40°C. (b)Relationship between near-infrared irradiation light
11 intensity and resistance with light intensity ranging from 0 to 0.485 mW, when the laser wavelength was 1530 nm. (c)
12 Relationship between light intensity and device temperature calculated using the results (a) and (b), and Eq. 4.

13

1

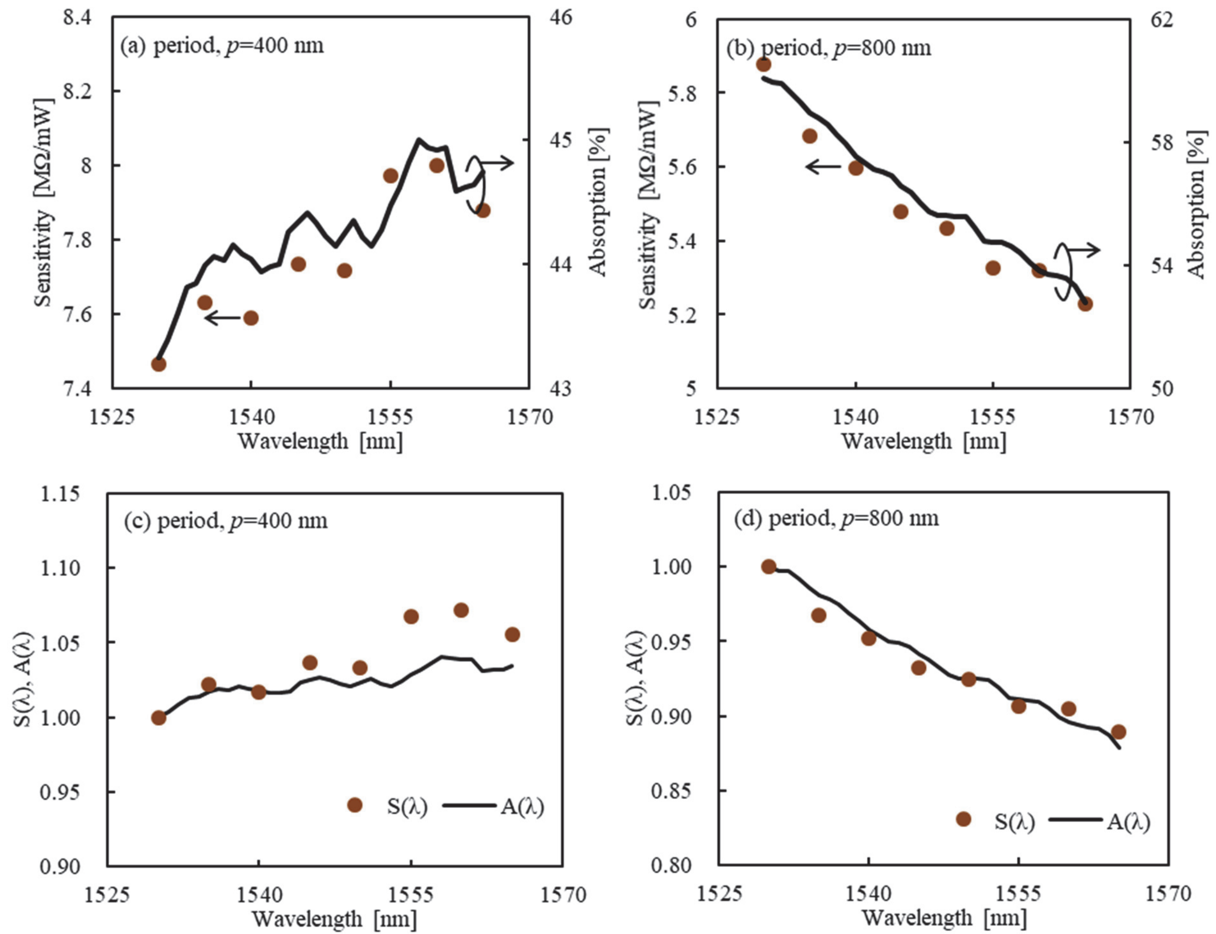

2
3
4 **Fig. 7** Wavelength-dependent responses. (a) Measured sensitivity and absorption with the grating period of 400 nm,
5 (b) Measured sensitivity and absorption with the grating period of 800 nm, (c) normalized sensitivity S(λ) and normalized
6 absorption A(λ) with the grating period of 400 nm, (d) normalized sensitivity S(λ) and normalized absorption A(λ) with
7 the grating period of 800 nm. The wavelength ranges from1530 to 1565 nm.
8